Ribonuclease-mediated control of body fat

Habacher, Cornelia; Guo, Yanwu; Venz, Richard; Kumari, Pooja; Neagu, Anca; Gaidatzis, Dimos; Harvald, Eva Bang; Færgeman, Nils J.; Gut, Heinz; Ciosk, Rafal

Published in:
Developmental Cell

DOI:
10.1016/j.devcel.2016.09.018

Publication date:
2016

Document version
Publisher's PDF, also known as Version of record

Citation for pulished version (APA):
Habacher, C., Guo, Y., Venz, R., Kumari, P., Neagu, A., Gaidatzis, D., ... Ciosk, R. (2016). Ribonuclease-mediated control of body fat. Developmental Cell, 39(3), 359-369. DOI: 10.1016/j.devcel.2016.09.018

Article

Developmental Cell

Ribonuclease-Mediated Control of Body Fat

Graphical Abstract

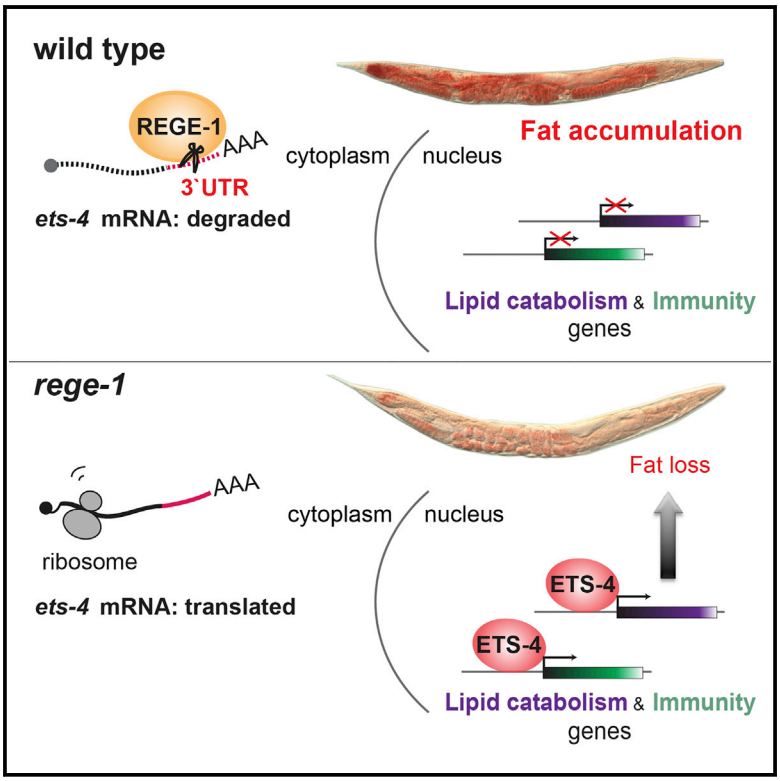

Highlights

- REGE-1, related to the RNase MCPIP1/Zc3h12a/Regnase-1, controls fat in *C. elegans*
- REGE-1 degrades mRNA encoding the transcription factor ETS-4
- ETS-4 induces expression of fat metabolic and defense genes
- REGE-1 and ETS-4 form a dynamic, auto-regulatory module controlling body fat

Authors

Cornelia Habacher, Yanwu Guo, Richard Venz, ..., Nils J. Færgeman, Heinz Gut, Rafal Ciosk

Correspondence

rafal.ciosk@fmi.ch

In Brief

Habacher et al. report that, in *C. elegans*, body fat is controlled by a module consisting of the RNase REGE-1 and its target, a fat-loss-promoting transcription factor. This dynamic, auto-regulatory model may be critical for rapid but reversible remodeling of metabolism for survival in the face of environmental change.

Habacher et al., 2016, Developmental Cell *39*, 359–369
November 7, 2016
http://dx.doi.org/10.1016/j.devcel.2016.09.018

CellPress

Developmental Cell
Article

Ribonuclease-Mediated Control of Body Fat

Cornelia Habacher,[1,2] Yanwu Guo,[1] Richard Venz,[1,2] Pooja Kumari,[1] Anca Neagu,[1] Dimos Gaidatzis,[1,4] Eva B. Harvald,[3] Nils J. Færgeman,[3] Heinz Gut,[1] and Rafal Ciosk[1,5,*]
[1]Friedrich Miescher Institute for Biomedical Research, Basel 4058, Switzerland
[2]University of Basel, Petersplatz 1, 4003 Basel, Switzerland
[3]Department of Biochemistry and Molecular Biology, University of Southern Denmark, Villum Center for Bioanalytical Sciences, 5230 Odense M, Denmark
[4]Swiss Institute of Bioinformatics, 4058 Basel, Switzerland
[5]Lead Contact
*Correspondence: rafal.ciosk@fmi.ch
http://dx.doi.org/10.1016/j.devcel.2016.09.018

SUMMARY

Obesity is a global health issue, arousing interest in molecular mechanisms controlling fat. Transcriptional regulation of fat has received much attention, and key transcription factors involved in lipid metabolism, such as SBP-1/SREBP, LPD-2/C/EBP, and MDT-15, are conserved from nematodes to mammals. However, there is a growing awareness that lipid metabolism can also be controlled by post-transcriptional mechanisms. Here, we show that the *Caenorhabditis elegans* RNase, REGE-1, related to MCPIP1/Zc3h12a/Regnase-1, a key regulator of mammalian innate immunity, promotes accumulation of body fat. Using exon-intron split analysis, we find that REGE-1 promotes fat by degrading the mRNA encoding ETS-4, a fat-loss-promoting transcription factor. Because ETS-4, in turn, induces *rege-1* transcription, REGE-1 and ETS-4 appear to form an auto-regulatory module. We propose that this type of fat regulation may be of key importance when, if faced with an environmental change, an animal must rapidly but precisely remodel its metabolism.

INTRODUCTION

Remodeling energy metabolism is critical for development, tissue homeostasis, and the etiology of numerous diseases including obesity and cancer (Folmes et al., 2012; Longo and Mattson, 2014; Ward and Thompson, 2012). Such remodeling can be induced by adverse environmental stimuli leading to a state of suspended animation or torpor. For example, hibernating animals use stored lipids, rather than carbohydrates, to fuel survival (Dark, 2005). In the wild, the *Caenorhabditis elegans* species populates temperate climates (Barrière and Félix, 2005), indicating that these animals are capable of surviving spells of cold. Indeed, when adapted to a decreasing temperature, *C. elegans* survives the exposure to near-freezing temperatures (Murray et al., 2007; Ohta et al., 2014).

In this study, we observed that *C. elegans* also utilize fat while in cold. Using cold sensitivity as the readout, we identified a putative RNase, REGE-1, related to the mammalian MCPIP1/Zc3h12a/Regnase-1, as a factor critical for *C. elegans* body fat accumulation. The examples of post-transcriptional regulation of fat remain few and are limited to specific microRNAs, whose functionally relevant mRNA targets remain, in most cases, unclear (Arner and Kulyté, 2015; Rottiers and Näär, 2012). In animals, microRNAs repress their mRNA targets through translational repression and/or exonucleolytic degradation (Wilczynska and Bushell, 2015). By contrast, MCPIP1 is a PIN-domain endonuclease (Iwasaki et al., 2011; Matsushita et al., 2009; Xu et al., 2012), suggesting a possible requirement for the endonucleolytic mRNA degradation in *C. elegans* body fat regulation. Indeed, we demonstrate that REGE-1 controls body fat by targeting the 3′ UTR of an mRNA encoding a fat-loss-promoting transcription factor, ETS-4. Interestingly, while REGE-1 inhibits ETS-4, ETS-4 promotes the expression of REGE-1. Such an auto-regulatory module is particularly well suited for a dynamic control of gene expression. It may be of key importance when, faced in the wild with an environmental change, an animal must rapidly remodel its fat metabolism to maximize its chances for survival.

RESULTS

Cold-Sensitivity Screen Reveals REGE-1 as a Factor Promoting Body Fat

Extending the initial observations by others that *C. elegans*, when adapted to a decreasing temperature, can survive exposure to near-freezing temperature (Murray et al., 2007; Ohta et al., 2014), we found that the animals can do so for many days, without a major impact on fecundity or lifespan (Figures S1A–S1C). To what degree the *C. elegans* response to cold is analogous to that of hibernating animals is not clear. Nevertheless, consistent with fueling cellular processes by fat in hibernators, we observed a gradual decline in the fat levels in "hibernating" *C. elegans* (Figure S1D). This observation prompted us to use cold sensitivity as a readout to uncover new regulators of fat stores. We performed a genome-wide RNAi screen, searching for genes essential at 4°C but non-essential at 20°C (Figure 1A). This approach uncovered factors implicated in diverse cellular processes (Figures 1B and S1E). Importantly,

A

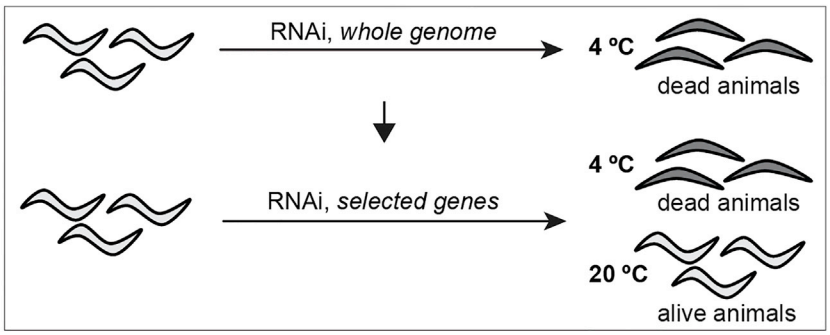

B

Gene	Molecular function	Human homologue
C30F12.1	Putative ribonuclease	ZC3H12A/B/C/D; Regnase-1
mdt-15	Mediator complex subunit	MED15; mediator of Pol II
vhp-1	MAPK Phosphatase, stress signaling	DUS16; dual spec. phosphatase 16
ptc-1	Predicted functions in protein, lipid and sterol transport	PTCH1; Patched homolog 1
paa-1	PP2A phosphatase structural subunit	PR65; Protein Phosphatase 2A, subunit A α isoform
inos-1	Predicted function in de novo inositol biosynthesis	ISYNA1; Inositol-3-phosphate synthase 1
pbs-6	Proteasome subunit	PSMB1; Proteasome sub. β type-1
R03E1.2	Unknown	ATP6AP2; Renin receptor
fat-6 & -7	Fatty acid desaturation	SCD; Acyl-CoA desaturase
R02F11.2	Unknown, nematode-specific	None

Figure 1. A Genome-wide RNAi Screen for Cold Sensitivity Uncovers a Conserved RNase as a Factor Promoting Accumulation of Body Fat

(A) Schematic description of the genome-wide RNAi screen for cold sensitivity. Only those RNAi clones that induced death following the incubation at 4°C, but not at 20°C, were investigated further. (B) Factors identified in the cold-sensitivity screen. Factors whose depletion results in "pale" animals, suggesting reduced fat levels, are shown in bold. This group includes a putative RNase, C30F12.1. See also Figure S1.

the depletion of several factors caused a "pale" appearance of animals already at 20°C, indicating reduced stores of body fat. Indeed, some of these factors have established roles in fat metabolism (Figure 1B). For example, the mediator complex component MDT-15 regulates expression of many fatty acid metabolism genes (Taubert et al., 2006), and FAT-6/-7 are fatty acid desaturases previously implicated in cold survival (Murray et al., 2007; Watts and Browse, 2000). In addition, knockdown of the hitherto uncharacterized gene *C30F12.1* resulted in pale animals. C30F12.1 protein is a member of the CCCH-type zinc-finger family (Liang et al., 2008) and is related to the mammalian MCPIP1/Zc3h12a/Regnase-1, a PIN-domain endonuclease (Xu et al., 2012), which directly degrades specific mRNAs such as those encoding pro-inflammatory cytokines (Iwasaki et al., 2011; Matsushita et al., 2009). Because the RNase and CCCH zinc-finger domains are highly conserved between C30F12.1 and Zc3h12a/MCPIP1/Regnase-1 (Figures S2 and 3A), we named C30F12.1 as REGE-1 (REGnasE-1). To verify that *C. elegans* lose fat upon *rege-1* RNAi, we stained the animals with oil red O and enzymatically determined the levels of triacylglycerides, which are the main storage form of lipids. By both approaches, we confirmed that the fat levels were reduced (Figures 2A and 2B). Additionally we examined lipid droplets in live animals by coherent anti-Stokes Raman spectroscopy (CARS) and found that REGE-1-depleted animals had substantially reduced numbers of lipid droplets (Figure 2C). Because germline plays an important role in fat homeostasis (Hansen et al., 2013), REGE-1 could affect body fat by functioning in the germline. However, the loss of fat also occurred in REGE-1-depleted, germline-less (*glp-1*) animals (Figure 2D), suggesting that, to promote fat accumulation, REGE-1 functions in the soma.

REGE-1 Is a Putative RNase Primarily Expressed in the Intestine

To study REGE-1 in more detail, we generated a deletion allele, *rege-1*(*rrr13*), predicted to cause a severe truncation of the protein (Figure 3A). Consistent with the RNAi-mediated depletion, *rege-1*(*rrr13*) animals were viable but displayed reduced fat (Figure 3B). We also observed that they developed somewhat slower than wild-type (Figure S3). Both of these phenotypes were rescued by a single-copy-integrated, GFP-tagged REGE-1, expressed under the control of endogenous promoter and 3′ UTR (Figures 3B and S3). This REGE-1::GFP was mostly expressed in the intestinal cells adjacent to the pharynx (Figure 3C), suggesting that REGE-1 functions in the intestine, the primary fat-storing organ of *C. elegans* (Srinivasan, 2014; Watts, 2009). Mammalian Regnase-1 is a cytoplasmic RNase that, by an internal cleavage, induces the degradation of specific mRNA targets (Iwasaki et al., 2011; Matsushita et al., 2009; Xu et al., 2012). Investigating the putative RNase domain of REGE-1, we noticed that the residues critical for the RNase activity of Regnase-1 are conserved in REGE-1 (Figures S2 and 3D), suggesting that REGE-1 may also function as an RNase.

REGE-1 Promotes Body Fat through the Transcription Factor ETS-4

Assuming that REGE-1 functions similarly to Regnase-1, depleting REGE-1 would be expected to primarily affect the levels of mature but not nascent transcripts. It has recently been shown that comparing exonic and intronic expression across conditions (exon-intron split analysis [EISA]) can be used to quantify the levels of nascent and mature transcripts in standard RNA-sequencing (RNA-seq) experiments (Gaidatzis et al., 2015). We thus performed RNA-seq on animals subjected to control or *rege-1* RNAi and compared changes in the levels of nascent RNAs (Δintron) with the changes in mRNAs (Δexon). Although most of the observed changes in

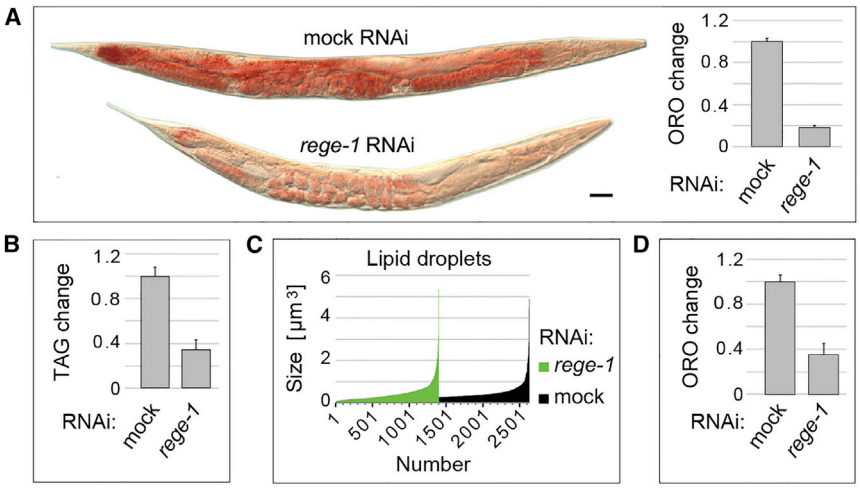

Figure 2. REGE-1 Promotes Fat Accumulation under Normal Growth Conditions

(A) Left: Differential interference contrast (DIC) color micrographs of animals, subjected to control (mock) or *rege-1* RNAi, stained with the lipophilic dye oil red O to reveal fat. Scale bar, 50 μm. Right: Quantification of changes in the oil red O staining. A total of 20–25 animals were measured per condition. Data are presented as mean; error bars, here and in all the subsequent graphs, represent SEM.

(B) Change in triacylglyceride levels upon *rege-1* RNAi.

(C) Size and numbers of lipid droplets quantified by CARS in control and *rege-1* RNAi-ed animals.

(D) Change in fat upon *rege-1* RNAi, in germlineless *glp-1*(*e2141*) animals, determined by the oil red O (ORO) staining. Ten to fifteen animals were measured per condition.

mRNA levels could be explained by differential transcription, we observed a small group of transcripts that were affected mainly at the level of mRNA, the most extreme example being *ets-4* mRNA (Figures 4A, 4B, and S4A; Tables S1 and S2). Consistent with REGE-1-mediated regulation, we found, by western blot, that the GFP- and FLAG-tagged ETS-4 protein was more abundant upon *rege-1* RNAi (Figure 4C). Importantly, we did not detect any obvious expression of this protein in wild-type animals, but observed its strong expression in the intestine nuclei upon *rege-1* knockdown (Figure 4C), suggesting that REGE-1 and ETS-4 function in the same tissue. ETS-4 belongs to the ETS-domain family of transcription factors (Sharrocks, 2001). Prior to this work, ETS-4 was studied in the context of aging and ETS-4-regulated genes were reported (Thyagarajan et al., 2010). Interestingly, we found that transcripts reportedly activated by ETS-4 were enriched among the transcripts upregulated in REGE-1-depleted animals (data not shown). This suggested the possibility that the increased expression of ETS-4 may be largely responsible for the changes in gene expression observed in *rege-1* animals. To test this, we compared changes in transcript levels between *rege-1*(*rrr13*) and *rege-1*(*rrr13*);*ets-4*(*RNAi*) animals with the changes in transcript levels between animals subjected to *rege-1* or mock RNAi. Impressively, we found that the majority of changes in gene expression observed in the absence of REGE-1 were reversed by the additional depletion of ETS-4 (Figure 4D and Table S3), suggesting that ETS-4 is the major effector of REGE-1. If so, the depletion of ETS-4 would be expected to rescue the phenotypes observed in *rege-1*(*rrr13*) animals. Indeed, we found that the RNAi-mediated depletion of *ets-4* mRNA (but not of other putative targets marked in red in Figure 4A) restored both fat and developmental timing in *rege-1*(*rrr13*) animals to the wild-type values (Figures 4E and S4B). By examining gene ontology terms associated with transcripts induced by ETS-4 in *rege-1*(*rrr13*) animals (the transcripts marked in red in Figure 4D), we found two major classes of genes: genes implicated in lipid metabolism and in responses to pathogens (Figure S5A and Table S4). While the former category includes key genes functioning in the fatty acid degradation pathway (Figure S5B), the latter category contains many genes induced upon infection with bacterial or fungal pathogens (Figure S5C) (Engelmann et al., 2011).

REGE-1 Regulates ETS-4 Post-transcriptionally through the 3′ UTR

Regnase-1 is an RNA-binding protein (RBP) that targets 3′ UTRs of specific mammalian mRNAs. To test whether REGE-1 regulates ETS-4 expression by targeting the 3′ UTR of *ets-4* mRNA, we produced strains carrying a single-copy-integrated *ets-4*::*gfp*, expressed from the endogenous *ets-4* promoter and fused to either endogenous (*ets-4*) or unregulated (*unc-54*) 3′ UTR. We found that the depletion of REGE-1 caused increased expression of ETS-4::GFP only when this expression was controlled by the *ets-4* 3′ UTR (Figure 5A). Thus, *ets-4* 3′ UTR is required for the REGE-1-mediated regulation. To examine this further, we produced a strain expressing a reporter GFP (fused to H2B to accumulate signal in the nucleus, facilitating quantification) from a ubiquitous promoter (*dpy-30*) under the control of the *ets-4* 3′ UTR. In wild-type animals, we observed the expression of this reporter in various tissues and across development (reflecting promoter activity, data not shown) but not in the gut nuclei (Figure 5B). In contrast, in *rege-1*(*rrr13*) mutants, this reporter GFP was additionally expressed in the gut nuclei (Figure 5B). Thus, the *ets-4* 3′ UTR is not only required but also sufficient for REGE-1-mediated regulation of ETS-4 expression. To examine which part of the *ets-4* 3′ UTR is targeted by REGE-1, we produced strains expressing the reporter GFP under the control of truncated variants of the *ets-4* 3′ UTR. We found that the fragment spanning the first one-third of the 3′ UTR (fragment F1, 357 nt) was sufficient for the repression of the reporter GFP in the gut nuclei and that this repression was alleviated upon *rege-1* RNAi (Figure 5C). Examining this fragment more closely, we noticed a stretch of homology between the corresponding sequences from other nematode species (Figure S6). To test the functional significance of this fragment (fragment F1S, 115 nt), we "transplanted" it into the otherwise unregulated *unc-54* 3′ UTR. We found that this transplantation rendered the *unc-54* 3′ UTR sensitive to the regulation by REGE-1 (Figure 5D), suggesting that the RNA features required for REGE-1-mediated regulation are contained within the F1S fragment.

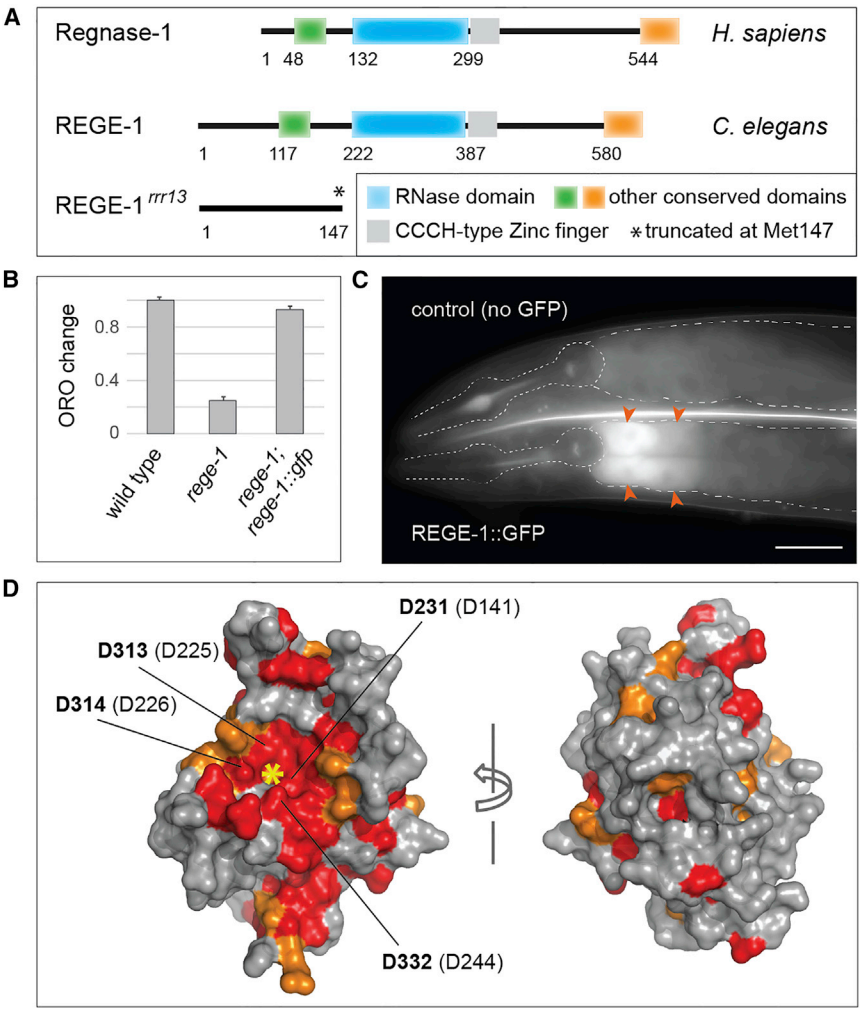

Figure 3. REGE-1 Is a Putative RNase Expressed in the Intestine

(A) Schematic view of Regnase-1/Zc3h12a/MCPIP1 and REGE-1 proteins, with the conserved domains indicated. The deletion allele of *rege-1*, *rege-1*(*rrr13*), results in a truncated protein missing the RNase domain.

(B) The fat-loss phenotype of animals subjected to *rege-1* RNAi is also observed in *rege-1*(*rrr13*) mutants, and is rescued by a transgenic GFP-tagged REGE-1. Fat levels were quantified with oil red O staining. Fifteen to twenty animals were measured per genotype.

(C) Partial view of representative live animals, either not expressing (upper animal) or expressing (lower animal) the rescuing REGE-1::GFP. To reduce gut-specific autofluorescence, the animals carried the *glo-1*(*zu391*) mutation (Hermann et al., 2005). The pharynx and intestines are outlined, and arrowheads point to the REGE-1::GFP-expressing intestinal cells adjacent to the pharynx. Scale bar, 50 μm.

(D) Homology model of the *C. elegans* REGE-1 RNase domain (surface representation), in two orientations, rotated around a vertical axis by 180°. Highly conserved residues computed by ConSurf (Glaser et al., 2003) are colored in red and orange (ConSurf color grades 9 and 8). Predicted active site (asterisk) and residues required for the RNase activity in the mammalian proteins are indicated. The numbers represent amino acid numbers in the *C. elegans* REGE-1 or, in parentheses, the human Regnase-1.

See also Figures S2 and S3.

REGE-1 Induces an Endonucleolytic Cleavage within the *ets-4* 3′ UTR

To test whether the putative RNase activity of REGE-1 is important for the regulation of *ets-4* mRNA, we mutated, by genome editing, conserved amino acids (indicated in Figure 3D) in the RNase domain of the endogenous REGE-1 (generating the *rrr21* allele of *rege-1*). As expected, mutating these residues (D231N, D313A, D314A, and D332A) resulted in increased levels of *ets-4* mRNA (Figure 6A). If REGE-1 is indeed an RNase, its association with *ets-4* mRNA is expected to be short lived. To examine this putative association, we used GFP-tagged and RNase domain-mutated REGE-1 (corresponding to the *rrr21* allele). By immunoprecipitating this REGE-1 variant, followed by qRT-PCR-based detection of associated transcripts, we observed that, indeed, REGE-1 associated with *ets-4* mRNA (Figure 6B). Based on the homology with Regnase-1 and the above experiments, REGE-1 is expected to induce an endonucleolytic cleavage within the F1S region of *ets-4* 3′ UTR. Initially, we tested this by incubating immunoprecipitates of GFP-tagged, wild-type, and RNase domain-mutated REGE-1 with in vitro-produced RNA, corresponding to the fragment F1S. We observed that the incubation with the wild-type, but not the RNase domain-mutated, REGE-1 resulted in the degradation of the F1S RNA, but had no effect on unrelated RNA (100 nt of *unc-54* 3′ UTR) (Figure 6C). Finally, although detecting mRNA cleavage intermediates can be difficult, we used a modified 5′ RACE (rapid amplification of 5′ complementary cDNA ends) approach to amplify the 3′-terminal cleavage intermediates of *ets-4* mRNA. Rewardingly, this approach revealed that REGE-1 cleaves *ets-4* mRNA within the F1S fragment of its 3′ UTR (Figure 6D).

REGE-1 and ETS-4 May Form a Dynamic, Auto-regulatory Module

One advantage of post-transcriptional gene regulation is its speed and reversibility. Thus, the REGE-1/ETS-4 axis is potentially well suited to dynamically control ETS-4 levels. To test the dynamics of ETS-4 expression, we examined *ets-4* mRNA levels during starvation, which was followed by refeeding. During starvation, *ets-4* mRNA levels remained low for several days, increasing somewhat on the sixth day (Figure 7A). In contrast, upon refeeding, *ets-4* levels were strongly increased. This increase was, however, transient, as the levels of *ets-4* were back to the pre-starvation values only 1 day after refeeding (Figure 7A). With the changing levels of *ets-4* mRNA, we expected to see the reciprocal changes in the levels of *rege*-1 mRNA. However, to our surprise we observed similar, rather than opposite, changes of *rege-1* and *ets-4* mRNAs (Figure 7A), suggesting their co-regulation. To test this further, we asked whether ETS-4

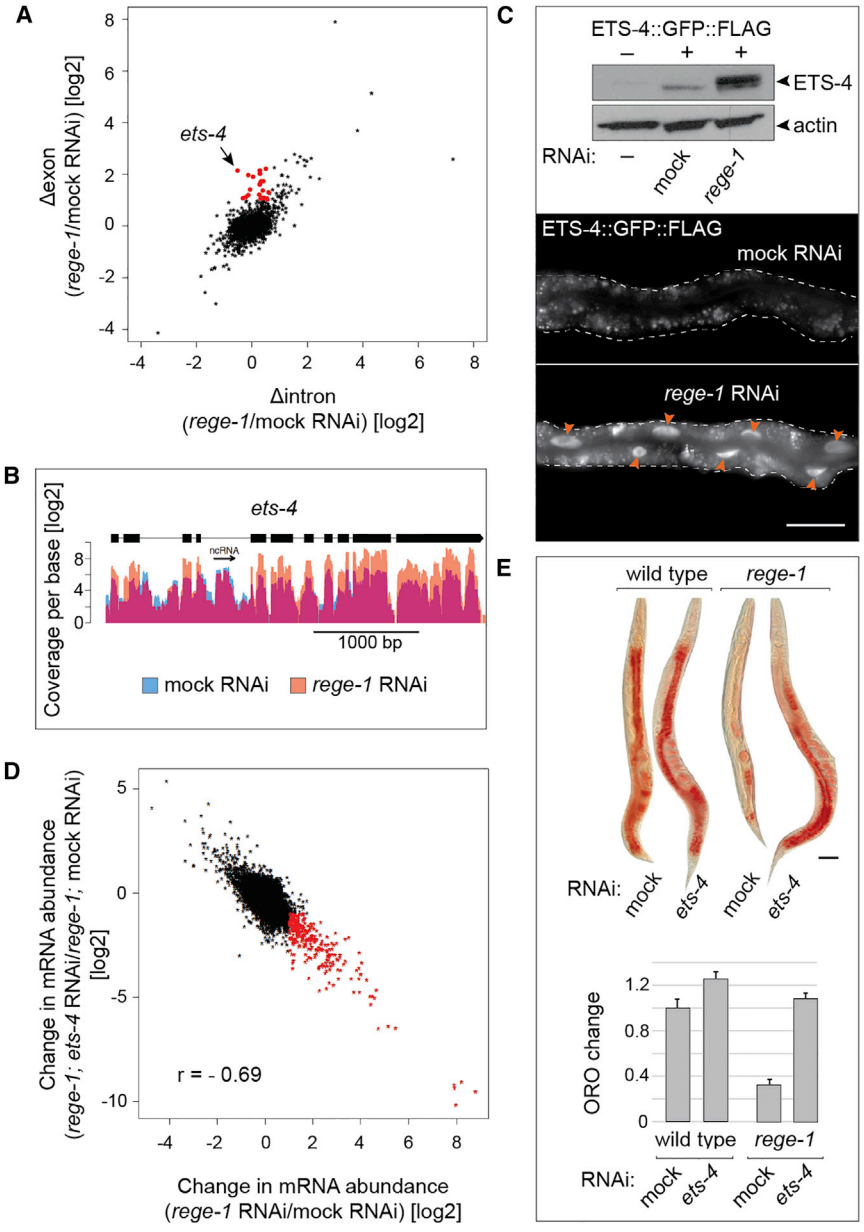

Figure 4. ETS-4 Is the Key Effector of REGE-1

(A) Plot comparing changes in the intronic (x = Δintron) versus exonic (y = Δexon) RNA-seq reads (reflecting changes in nascent versus mature transcripts, respectively) upon *rege-1* RNAi. The Pearson correlation of r = 0.61 suggests that a substantial part of the observed changes in mRNAs may be explained by differential transcription. Red: putative REGE-1 targets that predominantly change (more than 2-fold) in the exonic (mature mRNA) but not the intronic (nascent RNA) reads.

(B) RNA-seq read coverage at the genomic *ets-4* locus, from animals subjected to either control (blue) or *rege-1* (orange) RNAi. Exons are represented by thick lines and introns by thin lines. The arrow indicates an annotated non-coding RNA. The samples were normalized for read depth and two replicate experiments were combined to increase the coverage. Note the increase in the exonic (but not intronic) reads upon the depletion of REGE-1. Changes in the exonic and intronic reads are quantified in Figure S4A.

(C) Top: Western blot of extracts from animals expressing (+) or not expressing (–) tagged ETS-4 (ETS-4::GFP::FLAG), which were subjected to mock or *rege-1* RNAi. The abundance of ETS-4::GFP::FLAG (for brevity ETS-4), detected with anti-GFP antibody, increased upon *rege-1* RNAi. Actin was a loading control. Bottom: Partial view of live animals, subjected to mock or *rege-1* RNAi, with outlined intestines, expressing ETS-4::GFP::FLAG, visualized by GFP fluorescence. Arrowheads point to the gut nuclei in a representative *rege-1* RNAi-ed animal, all of which contain increased levels of ETS-4::GFP::FLAG. Scale bar, 20 μm.

(D) Plot comparing changes in transcript levels upon *rege-1* RNAi on otherwise wild-type animals (x axis) versus *ets-4* RNAi on *rege-1* mutant animals (y axis). Transcripts that were induced 2-fold by ETS-4 in *rege-1* animals are marked in red.

(E) Top: DIC color micrographs of representative wild-type and *rege-1*(*rrr13*) animals, subjected to either mock or *ets-4* RNAi, and stained by oil red O to visualize fat. Depleting ETS-4 restored fat in *rege-1* animals to the wild-type levels. Fifteen to twenty animals were measured per condition. Scale bar, 50 μm. Bottom: The corresponding oil red O quantifications.

See also Figures S4 and S5.

affects the levels of *rege-1* mRNA. Indeed, depleting ETS-4 resulted in reduced expression of *rege-1* (Figure 7B). We observed this effect also using a GFP reporter, driven from the *rege-1* promoter and under control of unregulated (*unc-54*) 3′ UTR (Figure 7C), suggesting that ETS-4 induces (directly or indirectly) the transcription of *rege-1*. Thus, our findings suggest that REGE-1 and ETS-4 form an auto-regulatory module, which, upon an environmental change, is capable of rapidly adjusting its transcriptional output by altering ETS-4 levels.

DISCUSSION

We describe here a previously uncharacterized RNase, REGE-1, involved in the regulation of body fat. The mammalian Regnase-1 binds mRNAs by recognizing structured RNA, reportedly with the help of a distinct RBP, Roquin (Jeltsch et al., 2014). However, Regnase-1 and Roquin have been recently suggested to function in distinct subcellular compartments and by different molecular mechanisms (Mino et al., 2015). Moreover, in addition to the RNase and zinc-finger domains, Regnase-1-like proteins contain two additional domains, of which one has been recently reported to contribute, at least in vitro, to the RNase activity of Regnase-1 (Yokogawa et al., 2016). Thus, the problems of how exactly Regnase-1-like proteins achieve specificity for selected mRNA targets and whether additional mechanisms contribute to mRNA regulation are only partly understood. Nevertheless, our results suggest that degradation, induced by an endonucleolytic cleavage, is

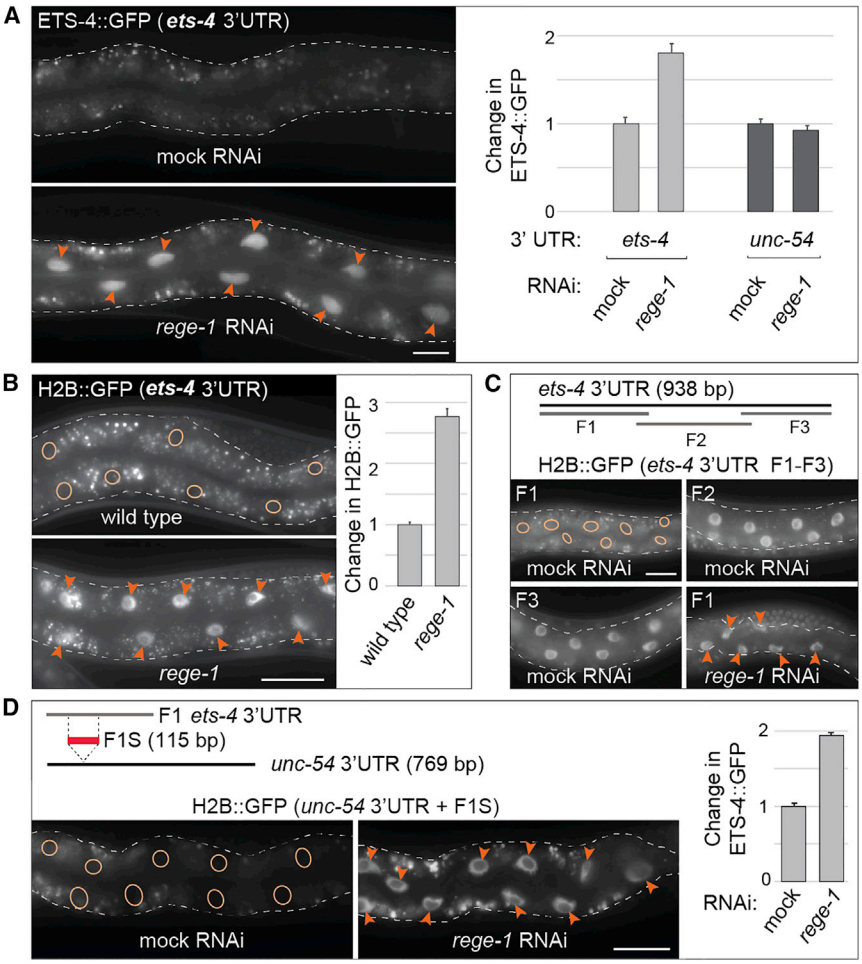

Figure 5. REGE-1 Controls ETS-4 Levels Post-transcriptionally

(A) Left: Partial view of live animals, with outlined intestines, expressing ETS-4::GFP from the endogenous *ets-4* promoter and under the control of *ets-4* 3′ UTR, subjected to either mock or *rege-1* RNAi. Arrowheads point to the gut nuclei expressing ETS-4::GFP. Scale bar, 20 μm. Right: The corresponding quantification of changes in the GFP intensity, including in the control animals expressing ETS-4::GFP under the control of unregulated *unc-54* 3′ UTR. The *ets-4*, but not *unc-54*, 3′ UTR rendered the expression of ETS-4::GFP sensitive to REGE-1. Between five and ten nuclei per animal, in at least five animals per condition, were analyzed. Error bars here and in subsequent panels represent SEM.

(B) Left: Partial view of live, wild-type, or *rege-1*(*rrr13*), animals, with outlined intestines, expressing GFP::H2B reporter from a ubiquitous promoter (*dpy-30*) under the control of *ets-4* 3′ UTR. Ovals in (B) to (D) indicate the positions of gut nuclei not expressing the reporter GFP in control animals. Arrowheads point to the gut nuclei expressing the reporter GFP in *rege-1* mutant (B) or *rege-1* RNAi-ed (C and D) animals. Scale bar, 50 μm. Right: The corresponding quantification of changes in the GFP intensity. Between five and ten nuclei per animal, in at least five animals per condition, were analyzed.

(C) Top: Schematic representation of the *ets-4* 3′ UTR and three tested fragments (F1–F3). Bottom: Partial view of representative live, wild-type animals, with outlined intestines, expressing the GFP::H2B reporter under the control of truncated *ets-4* 3′ UTRs. The animals were subjected to either mock or *rege-1* RNAi, as indicated. Only the F1 fragment of *ets-4* 3′ UTR caused repression of the GFP reporter. This repression was alleviated upon *rege-1* RNAi. Scale bar, 25 μm.

(D) Top: Schematic representation of the F1 fragment of the *ets-4* 3′ UTR and the shorter F1S fragment that was "transplanted" into an otherwise unregulated 3′ UTR (*unc-54*; the fragment was inserted between bp 164 and 165 of the 3′ UTR). Bottom: Partial view of live, wild-type animals, with outlined intestines, expressing the GFP::H2B reporter under the control of the modified *unc-54* 3′ UTR (containing the F1S fragment of *ets-4* 3′ UTR). The animals were subjected to either mock or *rege-1* RNAi, as indicated. Insertion of the F1S fragment into the *unc-54* 3′ UTR caused repression of the GFP reporter. This repression was alleviated upon *rege-1* RNAi. Scale bar, 25 μm. The corresponding quantification of changes in the GFP intensity is on the right. Between four and eight nuclei per animal, in at least eight animals per condition, were analyzed.

the most plausible mechanism by which REGE-1 controls *ets-4* mRNA.

While REGE-1 degrades *ets-4* mRNA, ETS-4 stimulates (directly or indirectly) the transcription of *rege-1*. Such an autoregulatory RNase/transcription factor module is well suited to a rapid and reversible regulation of gene expression. We hypothesize that, coupled to the positive transcriptional feedback, REGE-1-mediated degradation is more efficient at buffering changes in ETS-4 levels. Thus, upon an environmental cue, including but perhaps not limited to nutrient abundance, the reciprocal regulation of REGE-1 and ETS-4 might ensure a rapid but controlled change in the transcriptional output of ETS-4, eliciting desired metabolic remodeling (Figure 7D). However, proving this model will require quantitative measurements of both ETS-4 levels and ETS-4-induced transcription, upon manipulating regulatory elements in the *rege-1* promoter and *ets-4* 3′ UTR. Also, whether a particular environmental cue affects the module by primarily altering (levels or activity of) REGE-1 and/or ETS-4 will need to be established.

Finally, how precisely increased levels of ETS-4 stimulate fat loss remains an exciting problem for the future, with potential implications for obesity research. Our preliminary observations suggest that increased expression of ETS-4 does not alter feeding behavior, as monitored by pharyngeal pumping of *rege-1* mutants (our unpublished data). Therefore, the loss of fat is unlikely to be caused by reduced food consumption. Interestingly, upon refeeding (following long-term fasting), when the intestine is challenged with increased nutrient uptake and utilization, we observed a rapid upregulation of the REGE-1/ETS-4 module, possibly indicating a role for the module in accelerating food utilization. The observed induction of lipid genes by ETS-4, including genes in the fatty acid degradation pathway, is consistent with this hypothesis. Other scenarios are, however, possible. Whether the mammalian Regnase-1

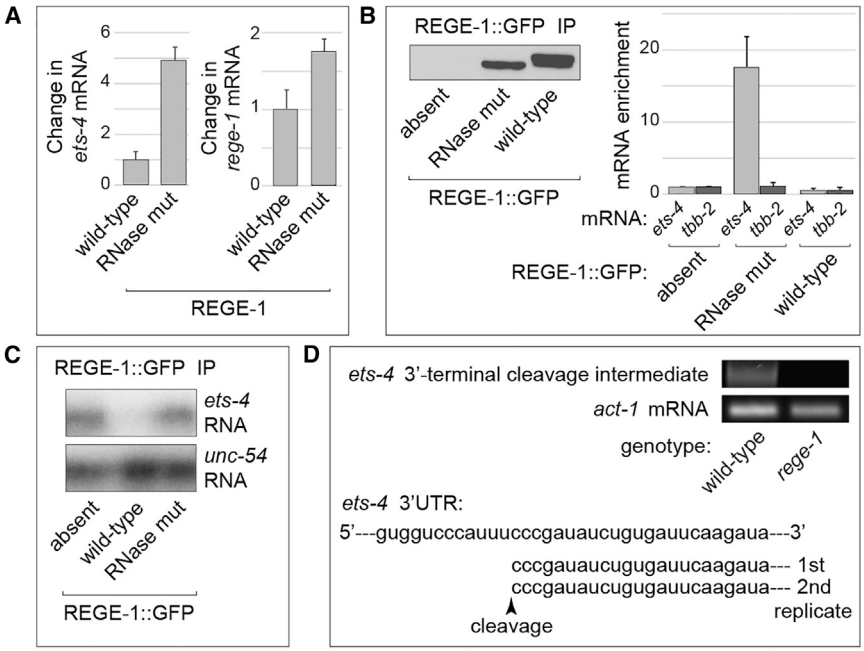

Figure 6. REGE-1 Induces an Endonucleolytic Cleavage within the *ets-4* 3′ UTR

(A) The levels of *ets-4* and *rege-1* mRNAs were measured, by qRT-PCR, in animals carrying either wild-type or mutated (RNase mut) alleles of *rege-1*. The RNase mut allele, *rege-1* (*rrr21*), was produced by changing four conserved residues in the RNase domain of REGE-1 (D231N, D313A, D314A, and D332A; see Figure 3D). Mutating these residues increased the levels of *ets-4* mRNA (left); this increase was not due to a lower expression of *rege-1* (right). The mRNA levels were normalized to the levels of *act-1* (actin) mRNA. Error bars here and in subsequent panels represent SEM.

(B) Extracts of wild-type animals, which either did not express GFP-tagged REGE-1, or expressed wild-type or the RNase mut GFP-tagged REGE-1, were subjected to immunoprecipitation (IP) using anti-GFP antibodies. Left: Western blot of the immunoprecipitates, showing that the RNase mut REGE-1::GFP was not expressed at a higher level than the wild-type. REGE-1::GFP was detected with REGE-1 antibody. Right: Quantification of the indicated mRNAs, by qRT-PCR, in the immunoprecipitates. As indicated by the enrichment of *ets-4* mRNA in the RNase mut REGE-1::GFP IP, REGE-1 associates with the *ets-4* mRNA.

(C) Immunoprecipitates, on beads, prepared as above, were incubated with labeled RNAs corresponding to either the F1S fragment of *ets-4* or a fragment of an unregulated (*unc-54*) 3′ UTR. Only wild-type REGE-1 induced the degradation of *ets-4* but not *unc-54* RNA.

(D) A modified 5′ RACE was performed to identify a 3′-terminal cleavage product of REGE-1 derived from the *ets-4* mRNA. Shown below is a partial sequence of F1S (beginning with nucleotide 89 of the *ets-4* 3′ UTR, indicated by the star in Figure S6) and sequences of two, independently amplified, 3′-terminal cleavage intermediates. Dashed lines represent sequences not shown for brevity.

See also Figure S6.

affects fat metabolism remains to be determined. In cultured adipocytes, where this possibility was addressed, the reported results are contradictory (Lipert et al., 2014; Younce et al., 2009). In contrast, in innate immune cells, Regnase-1 is well established to inhibit pro-inflammatory cytokines (Iwasaki et al., 2011; Matsushita et al., 2009) which, in turn, can stimulate adipocytes to lose fat (Gregor and Hotamisligil, 2011; Guilherme et al., 2008). Curiously, through ETS-4, REGE-1 regulates expression of many nematode defense genes, suggesting a conserved function of Regnase-1-like proteins in innate immunity. Although ETS-4 may control lipid and defense genes separately, perhaps depending on a particular environmental cue, it is possible that ETS-4-dependent fat loss is linked to an inflammatory response. If so, dissecting the underlying mechanism could provide important insights into the well-known, though insufficiently understood, connection between inflammation and lipid metabolism.

EXPERIMENTAL PROCEDURES

General Animal Handling and RNAi

Unless stated otherwise, animals were grown at 20°C as described previously (Brenner, 1974). RNAi of individual genes was performed by feeding animals with bacteria expressing double-stranded RNA, beginning from the L1 or L4 larval stage.

Genome-wide RNAi Screen

For the genome-wide RNAi screen we used the Ahringer feeding library. The library was replicated in the 96-well format. Overnight cultures of this stock, supplemented with 2 mM isopropyl β-D-1-thiogalactopyranoside, were used to seed 24-well plates. Ten to fifteen staged L4 N2 animals were transferred per well. Knockdown was conducted for about 40 hr and, after inspection for death or sterile animals, the animals were adapted at 10°C for 2 hr and then incubated at 4°C for 3 days. Afterward, the animals were incubated at 20°C for several hours to recover. Dead animals were scored and clones with more than four dead animals were retested at least three times. The RNAi clones were sequenced.

Oil Red O Staining, Image Processing, and Quantification

To visualize overall fat, we performed oil red O staining essentially as described previously (O'Rourke et al., 2009). All image-processing steps were carried out using the Fiji/ImageJ software suite (Schindelin et al., 2012). RGB images were stitched with the Grid/Collection stitching plug-in (Preibisch et al., 2009) and corrected for white balance by equalizing background mean values in the red, green, and blue channels. After conversion from RGB to HSB color space and background subtraction, red pixels were selected by thresholding the "H" (Hue) channel (only pixels with a Hue value between 0 and 7 are kept). A binary mask was created with the Saturation channel and applied to the thresholded image. After conversion to 32-bit, zero pixel values were replaced by NaN. The integrated density of all remaining pixels was used as an index of the amount of red staining in the animals (Fiji/ImageJ macro available upon request).

Triacylglyceride Assay

Total triacylglyceride content was assayed essentially as described previously (Martorell et al., 2012), using the Triglyceride Quantification Colorimetric/Fluorometric Kit from Biovision (catalog no. K622-100). Animals were synchronized by hypochlorite treatment and grown on OP50 plates at 20°C to the L4 stage. RNAi knockdown was performed for 48 hr. After collecting 50 animals, and two washes in PBS, the animals were pelleted and resuspended in 300 μL of triacylglyceride buffer. Sonication was conducted with a Branson Digital Sonifier five times at 10% power for 30 s. Worm debris were excluded by centrifugation and supernatant heated twice to 95°C for 5 min. Amounts of the supernatant (50 and 25 μL) were used to assess triacylglyceride content according to the

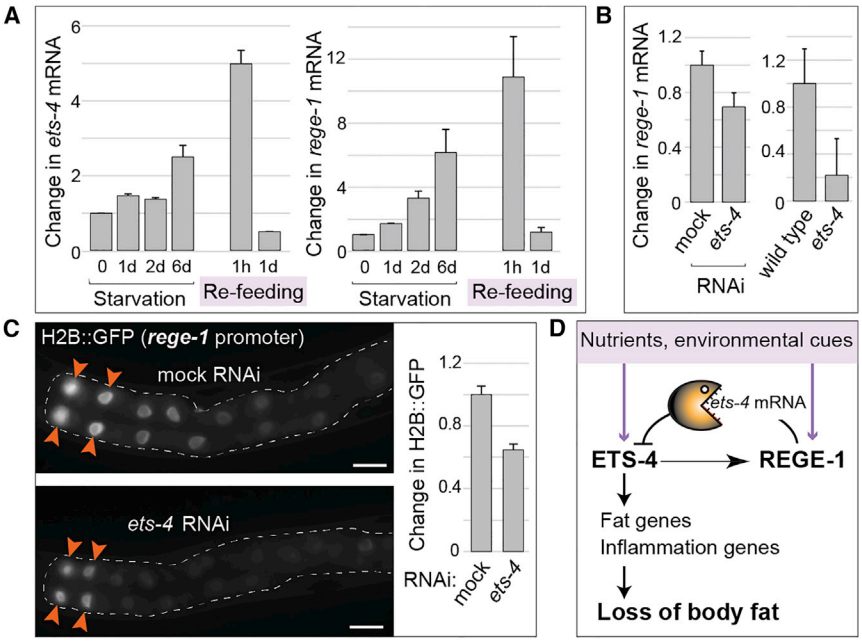

Figure 7. REGE-1 and ETS-4 Form an Autoregulatory Module

(A) Left: The levels of *ets-4* mRNA were measured, at indicated time points, by qRT-PCR, in wild-type animals subjected to starvation for 6 days, which was followed by refeeding for 1 day. Right: The corresponding changes in the levels of *rege-1* mRNA. The mRNA levels, here and in (B), were normalized to the levels of *act-1* mRNA. Error bars here and in subsequent panels represent SEM.

(B) The levels of *rege-1* mRNAs were measured, by qRT-PCR, in animals subjected to either control or *ets-4* RNAi (left), and in wild-type or *ets-4*(*rrr16*) mutants (right).

(C) Left: Representative fluorescent micrographs of intestines (outlined), expressing GFP::H2B reporter from the *rege-1* promoter, under the control of unregulated (*unc-54*) 3′ UTR. The promoter was mostly induced in the first two pairs of intestinal cells (arrowheads). Upon *ets-4* RNAi, this expression was reduced. Scale bar, 20 μm. Right: The corresponding quantification of changes in the GFP intensity. Nuclei from the first two pairs of the intestinal cells, in five animals, were analyzed.

(D) A model for the REGE-1/ETS-4-mediated control of body fat. An environmental change, such as nutrient availability, is transmitted, by yet unknown mechanism(s), to alter the level of ETS-4 and/or REGE-1. Because REGE-1 inhibits ETS-4 (by degrading *ets-4* mRNA) and, conversely, ETS-4 promotes REGE-1 (by inducing, directly or indirectly, *rege-1* transcription), a change in either protein eventually alters the abundance of ETS-4. This leads to altered expression of ETS-4 target genes, including fat catabolic and innate immunity genes, consequently leading to either gain (when ETS-4 is low) or loss (when ETS-4 is high) of fat.

protocol provided with the kit. Measurements were done in biological triplicates and technical duplicates.

Coherent Anti-Stokes Raman Spectroscopy

Animals were grown at 20°C from L1 to L4 stage and then transferred to RNAi plates. After 48 hr, animals were mounted on a slide with a drop of 2% agarose with 20 mM levamisol. The animals were then examined by CARS microscopy on a Leica TCS SP8 system with a CARS laser picoEmerald (optical parametric oscillator, >600 mW at 780–940 nm, pulse width 5–6 ps, 80 MHz; pump, >750 mW at 1,064 nm, pulse length 7 ps, 80 MHz) and with LAS AF software. The lasers were adapted to the symmetrical C-H stretch range by tuning the pump beam to 816.4 nm while keeping the Stokes beam constant at 1,064.6 nm. The output of both lasers was set to 1.3 W and the scan speed to 400 Hz. An image with the dimensions 145.31 × 145.31 μm (968 × 968 pixels) and stacks of approximately 30–50 sections with a step size of approximately 0.6 μm were collected. Only signals from epi-CARS (E-CARS) and epi-SHG (E-SHG) detectors were collected. Animals were imaged just below the pharynx with one stack per animal and approximately ten animals per condition. Each experiment was repeated three times. The number and size of lipid droplets in each stack were examined with the Fiji software package with the plug-in DropletFinder.

Homology Modeling of *C. elegans* REGE-1 RNase Domain

The protein sequence of the REGE-1 RNase domain (Uniprot: Q95YE2) was submitted to the HHPRED server for homology detection and structure prediction (Söding et al., 2005) in a search against known structures in the PDB (www.rcsb.org). The structure of the human Regnase-1/MCPIP1 RNase domain (PDB: 3V33 [Xu et al., 2012]) was the top hit (score = 360.7, E value = 2.9×10^{-57}, 60% sequence identity), and its HHPRED alignment with the REGE-1 RNase domain was used for calculating a homology model encompassing residues 224–384 via the HHPRED MODELLER pipeline. Structural figures were prepared with PyMOL (www.pymol.org).

Mapping of Conservation onto the REGE-1 RNase Domain Homology Model

The homology model of REGE-1 RNase domain (residues 224–384) was uploaded to the ConSurf server (Glaser et al., 2003) using default parameters for mapping of conserved residues onto the structural model. The PSI-BLAST search for homologous sequences was done against the UniProt database and position-specific conservation scores were calculated on 100 unique sequences.

Developmental Timing Assay

Animals were synchronized by bleaching and allowed to hatch in M9 buffer overnight. Around 200 staged L1 animals of each genotype were allowed to develop into L4s on RNAi knockdown and control plates. Picking L4s, the ratio of young adults/L4 (at least 35 animals per time point) was assessed every 2–3 hr until all animals, of the respective strains, had reached adulthood. Development of vulva, alae, and gonad were used to judge the developmental stage.

RNA Extraction, RNA-Seq, and Genomic Data

Frozen pellets of about 6,000 staged, young adults were subjected to RNA extraction with TRIzol as described previously (Arnold et al., 2014). Subsequently, RNA was depleted of rRNA using the Ribo-Zero Magnetic Kit (MRZ11124C) from epicenter and column purified with the RNA Cleanup & Concentrator from Zymo Research. Quality of RNA was monitored by Bioanalyzer RNA Pico chip. The library was prepared using the ScriptSeq v2 RNA-Seq Library Preparation Kit (Epicentre).

Gene expression levels (exonic) from RNA-seq data were quantified as described previously (Hendriks et al., 2014). After normalization for library size, $\log_2$ expression levels were calculated after adding a pseudocount of 8 ($y = \log_2[x + 8]$). The *rege-1* and *ets-4* RNAi experiments were normalized separately. Intronic expression levels were quantified as previously described (Gaidatzis et al., 2015). EISA was performed for a subset of genes (n = 3,093) that showed an average expression level (considering all samples) of at least 4.5 on the exonic as well as the intronic level. Genes (n = 283) both upregulated upon *rege-1* RNAi and downregulated upon *ets-4* RNAi were subjected to gene ontology over-representation analysis using the PANTHER classification system (Mi et al., 2005) with default settings.

The genomic data have been deposited at the GEO with accession number GEO: GSE75163. See also Tables S1, S2, and S3.

qRT-PCR

RNA for qRT-PCR was extracted as described above. Three hundred nanograms of RNA was used for reverse transcription utilizing the QuantiTect Reverse Transcription Kit (Qiagen). The resulting cDNA was diluted 1:10 for further analysis. Five microliters of this dilution was used with equal volume of Express SYBR GreenER qPCR SuperMix w/ROX (Invitrogen) containing 0.2 μL of 10 mM gene-specific primers. The StepOne RT-PCR system combined with StepOne Software (Applied Biotechnologies) was used for analysis. The presented values are based on three biological replicates.

Western Blot Analysis

Western blot analysis was conducted as described previously (Arnold et al., 2014). Primary antibodies diluted in 4% milk/PBS-Tween 20 were mouse α-ACT-1 (1:2,000; MAB1501, Millipore) and mouse α-GFP (1:1,000; Roche). Secondary antibodies were horseradish peroxidase-coupled α-mouse (1:4,000; GM Healthcare), and the REGE-1 polyclonal rabbit antibody was raised against the first 119 amino acids (SDIX), used at 1:1,000.

Generation of *rege-1*(*rrr13*) and *ets-4*(*rrr16*) Alleles, GFP-Tagged REGE-1 and ETS-4, and GFP Reporter Lines

The *rege-1*(*rrr13*) and *ets-4*(*rrr16*) alleles were generated by CRISPR/Cas9 (Arribere et al., 2014; Katic et al., 2015). The mutations were verified by sequencing and outcrossed six times before analyzing. The ETS-4::GFP, REGE-1::GFP, and 3′ UTR reporter lines were constructed by MosSCI (Frøkjaer-Jensen et al., 2008). In constructing the *ets-4*::*gfp*, we used the *ets-4* promoter sequence (2,634 bp), *ets-4* genomic sequence fused to the gfp, and the *ets-4* 3′ UTR (938 bp). In constructing the *rege-1*::*gfp*, the promoter sequence (2,989 bp) was fused to *rege-1* cDNA (1,908 bp), *gfp*, and *rege-1* 3′ UTR (262 bp). To check whether the F1S sequence is sufficient for REGE-1-mediated regulation, we inserted it into an otherwise unregulated 3′ UTR, *unc54*, between bp 164 and 165. The single guide RNA sequences and primers used for construct generation are provided in Supplemental Experimental Procedures.

Quantification of the ETS-4 3′ UTR GFP Reporter

Images for quantification of GFP intensity of reporter strains were acquired with an AxioImager.Z1 microscope (Zeiss) equipped with a 63× objective and an MRm camera (Zeiss). Signal intensity of a circular area of 52-pixels diameter of five to seven gut nuclei from five animals per condition was measured in ImageJ and normalized to the background. In addition, 30–35 animals per strain were visually inspected for GFP expression.

Generation of Point Mutations in the REGE-1 RNase Domain

Four point mutations (D231N, D313A, D314A, and D332A) were introduced at the endogenous locus of *C30F12.1*, by CRISPR/Cas9 genome editing performed by Knudra Transgenics. The editing was performed in two steps: in the first D231N and then, simultaneously, D313A, D314A, and D332A. The obtained mutations, resulting in the *rege-1*(*rrr21*) allele, were verified by sequencing and the homozygous quadruple mutant was outcrossed three times to the wild-type.

Starvation and Refeeding

The assay was modified after Seidel and Kimble (2011). Animals synchronized by hypochloride treatment were hatched overnight in M9 and grown to young L4 stage. They were collected, washed two times with M9 buffer, and transferred to plates devoid of bacteria. For refeeding, the animals were transferred to bacteria-seeded plates. At indicated times, RNA was extracted and processed as described earlier.

REGE-1 Immunoprecipitation/ETS-4 qRT-PCR

Proteins were extracted from staged young adults as described for western blot analysis. Forty microliters of Chromotek GFP Trap_A was washed twice in EB++ (EB + RNasin 5 μL/ml from Promega) and 3 mg of protein was added to a final volume of 1 mL. After incubation overnight on 4°C, the beads were washed four times with 600 μL of EB++ and RNA was extracted directly from the beads by adding 500 μL of TRIzol. After RNA extraction and subsequent qPCR analysis, fold enrichment was calculated as follows: Enrichment RNA immunoprecipitation (RIP) over input: ΔCt [normalized RIP] = Ct [RIP] − (Ct[input] − $\log_2$(input dilution factor)); normalized to control/non-specific (NS) IP ΔΔCt [RIP/NS] = ΔCt [normalized RIP] − Δ [normalized NS]; fold enrichment: $2^{-\Delta\Delta Ct}$ [RIP/NS].

On-the-Beads RNase Assay

Radioactively labeled RNAs were transcribed from PCR products. Templates for transcription were generated by PCR with an extended phage T3 RNA polymerase promoter (AATTAACCCTCACTAAAGGGAGAA) appended to the 5′ end of the 5′ primer, and gel purified. Transcription was performed in 3-μL reactions containing 0.5 μL of template, 1.5 μL of αP32 UTP (3 μM), and 0.6 μL of 5× transcription buffer (Promega), 0.2 μL of RNasin (Promega), and 2.5 mM rATP, 2.5 mM rGTP, 2.5 mM rCTP, and 0.025 mM rUTP (adenosine, guanidine, cytidine, and uridine triphosphates; Roche) at 37°C for 3 hr. The reaction was stopped by adding 30 μL of Tris-EDTA and the RNA was purified on Sephadex G-25 columns (Roche) using the manufacturer's instructions. REGE-1::GFP was immunoprecipitated as described above. The beads were washed additionally once with RNase assay buffer (20 mM Tris-HCl [pH 7.5], 150 mM NaCl, 5 mM $MgCl_2$, 2 mM DTT). RNA (10^5 cpm) was suspended in RNase assay buffer and incubated with immunoprecipitation beads for 15 min at room temperature. The tubes were centrifuged and the supernatant loaded on a pre-run 6% denaturing polyacrylamide gel. After electrophoresis at 200 V for 90 min, the gel was dried and auto-radiographed.

Modified 5′ RACE

To identify the 3′-terminal cleavage product of *ets-4* mRNA, we employed a modified 5′ RLM RACE protocol (Schmidt et al., 2015). Total RNA (3–5 μg) was ligated with 0.8 μg of 5′ RNA linker (GUUCAGAGUUCUACAGUCCGACGAUC) in a 10-μL reaction with 5 U of T4 RNA ligase in 1× RNA ligase buffer (NEB) and 1.5 mM ATP. The ligated RNA sample was reverse transcribed with a gene-specific primer for *ets-4* and SuperscriptIII reverse transcriptase (Thermo Fischer Scientific) using the manufacturer's instructions. PCR was performed to obtain the cleaved product using a forward primer in 5′ RNA linker and *ets-4* reverse primer upstream of the RT primer. PCR products were sequenced to determine the cleavage site.

ACCESSION NUMBERS

The WormBase ID for the gene *C30F12.1* is: WBGene00016260.

SUPPLEMENTAL INFORMATION

Supplemental Information includes Supplemental Experimental Procedures, six figures, and four tables and can be found with this article online at http://dx.doi.org/10.1016/j.devcel.2016.09.018.

AUTHOR CONTRIBUTIONS

R.C. wrote the manuscript and designed the experiments. C.H. designed and performed the majority of the experiments. Y.G. constructed *ets-4* transgenic lines, demonstrated the regulation of *rege-1* by ETS-4, and helped in analyzing the genomic data. R.V. performed the initial cold-sensitivity screen and analysis. P.K. assisted with the 5′ RACE and on-beads RNase assay. A.N. assisted with constructing some transgenic strains. D.G. analyzed the RNA-seq data. E.B.H. and N.J.F. performed the CARS experiment. H.G. did homology analysis and modeling of the *C. elegans* RNase domain. All authors contributed to interpretation of the data and provided comments on the manuscript.

ACKNOWLEDGMENTS

We thank Hugo Aguilaniu and Witold Filipowicz for comments on the manuscript, members of the Ciosk laboratory for discussions, Iskra Katic for technical help, and Laurent Gelman for help with oil red O quantification. Some of the strains were provided by the Caenorhabditis Genetics Center (CGC) funded by the NIH. P.K. has received funding for the research leading to these results from the EMBO Fellowship (ALTF 95-2015) co-funded by the European Commission support for Marie Curie Actions (LTFCOFUND2013, GA-2013-609409). FMI is sponsored by the Novartis Research Foundation.

Received: March 25, 2016
Revised: June 27, 2016
Accepted: September 16, 2016
Published: October 13, 2016

REFERENCES

Arner, P., and Kulyté, A. (2015). MicroRNA regulatory networks in human adipose tissue and obesity. Nat. Rev. Endocrinol. *11*, 276–288.

Arnold, A., Rahman, M.M., Lee, M.C., Muehlhaeusser, S., Katic, I., Gaidatzis, D., Hess, D., Scheckel, C., Wright, J.E., Stetak, A., et al. (2014). Functional characterization of *C. elegans* Y-box-binding proteins reveals tissue-specific functions and a critical role in the formation of polysomes. Nucleic Acids Res. *42*, 13353–13369.

Arribere, J.A., Bell, R.T., Fu, B.X.H., Artiles, K.L., Hartman, P.S., and Fire, A.Z. (2014). Efficient marker-free recovery of custom genetic modifications with CRISPR/Cas9 in *Caenorhabditis elegans*. Genetics *198*, 837–846.

Barrière, A., and Félix, M.-A. (2005). Natural variation and population genetics of *Caenorhabditis elegans*. WormBook, 1–19.

Brenner, S. (1974). The genetics of *Caenorhabditis elegans*. Genetics *77*, 71–94.

Dark, J. (2005). Annual lipid cycles in hibernators: integration of physiology and behavior. Annu. Rev. Nutr. *25*, 469–497.

Engelmann, I., Griffon, A., Tichit, L., Montañana-Sanchis, F., Wang, G., Reinke, V., Waterston, R.H., Hillier, L.W., and Ewbank, J.J. (2011). A comprehensive analysis of gene expression changes provoked by bacterial and fungal infection in *C. elegans*. PLoS One *6*, e19055.

Folmes, C.D.L., Dzeja, P.P., Nelson, T.J., and Terzic, A. (2012). Metabolic plasticity in stem cell homeostasis and differentiation. Cell Stem Cell *11*, 596–606.

Frøkjaer-Jensen, C., Davis, M.W., Hopkins, C.E., Newman, B.J., Thummel, J.M., Olesen, S.-P., Grunnet, M., and Jorgensen, E.M. (2008). Single-copy insertion of transgenes in *Caenorhabditis elegans*. Nat. Genet. *40*, 1375–1383.

Gaidatzis, D., Burger, L., Florescu, M., and Stadler, M.B. (2015). Analysis of intronic and exonic reads in RNA-seq data characterizes transcriptional and post-transcriptional regulation. Nat. Biotechnol. *33*, 722–729.

Glaser, F., Pupko, T., Paz, I., Bell, R.E., Bechor-Shental, D., Martz, E., and Ben-Tal, N. (2003). ConSurf: identification of functional regions in proteins by surface-mapping of phylogenetic information. Bioinformatics *19*, 163–164.

Gregor, M.F., and Hotamisligil, G.S. (2011). Inflammatory mechanisms in obesity. Annu. Rev. Immunol. *29*, 415–445.

Guilherme, A., Virbasius, J.V., Puri, V., and Czech, M.P. (2008). Adipocyte dysfunctions linking obesity to insulin resistance and type 2 diabetes. Nat. Rev. Mol. Cell Biol. *9*, 367–377.

Hansen, M., Flatt, T., and Aguilaniu, H. (2013). Reproduction, fat metabolism, and life span: what is the connection? Cell Metab. *17*, 10–19.

Hendriks, G.-J., Gaidatzis, D., Aeschimann, F., and Grosshans, H. (2014). Extensive oscillatory gene expression during *C. elegans* larval development. Mol. Cell *53*, 380–392.

Hermann, G.J., Schroeder, L.K., Hieb, C.A., Kershner, A.M., Rabbitts, B.M., Fonarev, P., Grant, B.D., and Priess, J.R. (2005). Genetic analysis of lysosomal trafficking in *Caenorhabditis elegans*. Mol. Biol. Cell *16*, 3273–3288.

Iwasaki, H., Takeuchi, O., Teraguchi, S., Matsushita, K., Uehata, T., Kuniyoshi, K., Satoh, T., Saitoh, T., Matsushita, M., Standley, D.M., and Akira, S. (2011). The IκB kinase complex regulates the stability of cytokine-encoding mRNA induced by TLR-IL-1R by controlling degradation of regnase-1. Nat. Immunol. *12*, 1167–1175.

Jeltsch, K.M., Hu, D., Brenner, S., Zöller, J., Heinz, G.A., Nagel, D., Vogel, K.U., Rehage, N., Warth, S.C., Edelmann, S.L., et al. (2014). Cleavage of roquin and regnase-1 by the paracaspase MALT1 releases their cooperatively repressed targets to promote TH17 differentiation. Nat. Immunol. *15*, 1079–1089.

Katic, I., Xu, L., and Ciosk, R. (2015). CRISPR/Cas9 genome editing in *Caenorhabditis elegans*: evaluation of templates for homology-mediated repair and knock-ins by homology-independent DNA repair. G3 (Bethesda) *5*, 1649–1656.

Liang, J., Wang, J., Azfer, A., Song, W., Tromp, G., Kolattukudy, P.E., and Fu, M. (2008). A novel CCCH-zinc finger protein family regulates proinflammatory activation of macrophages. J. Biol. Chem. *283*, 6337–6346.

Lipert, B., Wegrzyn, P., Sell, H., Eckel, J., Winiarski, M., Budzynski, A., Matlok, M., Kotlinowski, J., Ramage, L., Malecki, M., et al. (2014). Monocyte chemoattractant protein-induced protein 1 impairs adipogenesis in 3T3-L1 cells. Biochim. Biophys. Acta *1843*, 780–788.

Longo, V.D., and Mattson, M.P. (2014). Fasting: molecular mechanisms and clinical applications. Cell Metab. *19*, 181–192.

Martorell, P., Llopis, S., González, N., Montón, F., Ortiz, P., Genovés, S., and Ramón, D. (2012). *Caenorhabditis elegans* as a model to study the effectiveness and metabolic targets of dietary supplements used for obesity treatment: the specific case of a conjugated linoleic acid mixture (Tonalin). J. Agric. Food Chem. *60*, 11071–11079.

Matsushita, K., Takeuchi, O., Standley, D.M., Kumagai, Y., Kawagoe, T., Miyake, T., Satoh, T., Kato, H., Tsujimura, T., Nakamura, H., and Akira, S. (2009). Zc3h12a is an RNase essential for controlling immune responses by regulating mRNA decay. Nature *458*, 1185–1190.

Mi, H., Lazareva-Ulitsky, B., Loo, R., Kejariwal, A., Vandergriff, J., Rabkin, S., Guo, N., Muruganujan, A., Doremieux, O., Campbell, M.J., et al. (2005). The PANTHER database of protein families, subfamilies, functions and pathways. Nucleic Acids Res. *33*, D284–D288.

Mino, T., Murakawa, Y., Fukao, A., Vandenbon, A., Wessels, H.-H., Ori, D., Uehata, T., Tartey, S., Akira, S., Suzuki, Y., et al. (2015). Regnase-1 and roquin regulate a common element in inflammatory mRNAs by spatiotemporally distinct mechanisms. Cell *161*, 1058–1073.

Murray, P., Hayward, S.A.L., Govan, G.G., Gracey, A.Y., and Cossins, A.R. (2007). An explicit test of the phospholipid saturation hypothesis of acquired cold tolerance in *Caenorhabditis elegans*. Proc. Natl. Acad. Sci. USA *104*, 5489–5494.

O'Rourke, E.J., Soukas, A.A., Carr, C.E., and Ruvkun, G. (2009). *C. elegans* major fats are stored in vesicles distinct from lysosome-related organelles. Cell Metab. *10*, 430–435.

Ohta, A., Ujisawa, T., Sonoda, S., and Kuhara, A. (2014). Light and pheromone-sensing neurons regulates cold habituation through insulin signalling in *Caenorhabditis elegans*. Nat. Commun. *5*, 4412.

Preibisch, S., Saalfeld, S., and Tomancak, P. (2009). Globally optimal stitching of tiled 3D microscopic image acquisitions. Bioinformatics *25*, 1463–1465.

Rottiers, V., and Näär, A.M. (2012). MicroRNAs in metabolism and metabolic disorders. Nat. Rev. Mol. Cell Biol. *13*, 239–250.

Schindelin, J., Arganda-Carreras, I., Frise, E., Kaynig, V., Longair, M., Pietzsch, T., Preibisch, S., Rueden, C., Saalfeld, S., Schmid, B., et al. (2012). Fiji: an open-source platform for biological-image analysis. Nat. Methods *9*, 676–682.

Schmidt, S.A., Foley, P.L., Jeong, D.-H., Rymarquis, L.A., Doyle, F., Tenenbaum, S.A., Belasco, J.G., and Green, P.J. (2015). Identification of SMG6 cleavage sites and a preferred RNA cleavage motif by global analysis of endogenous NMD targets in human cells. Nucleic Acids Res. *43*, 309–323.

Seidel, H.S., and Kimble, J. (2011). The oogenic germline starvation response in *C. elegans*. PLoS One *6*, e28074.

Sharrocks, A.D. (2001). The ETS-domain transcription factor family. Nat. Rev. Mol. Cell Biol. *2*, 827–837.

Söding, J., Biegert, A., and Lupas, A.N. (2005). The HHpred interactive server for protein homology detection and structure prediction. Nucleic Acids Res. *33*, W244–W248.

Srinivasan, S. (2014). Regulation of body fat in *Caenorhabditis elegans*. Annu. Rev. Physiol. *77*, 161–178.

Taubert, S., Van Gilst, M.R., Hansen, M., and Yamamoto, K.R. (2006). A Mediator subunit, MDT-15, integrates regulation of fatty acid metabolism by NHR-49-dependent and -independent pathways in *C. elegans*. Genes Dev. *20*, 1137–1149.

Thyagarajan, B., Blaszczak, A.G., Chandler, K.J., Watts, J.L., Johnson, W.E., and Graves, B.J. (2010). ETS-4 is a transcriptional regulator of life span in *Caenorhabditis elegans*. PLoS Genet. *6*, e1001125.

Ward, P.S., and Thompson, C.B. (2012). Metabolic reprogramming: a cancer hallmark even Warburg did not anticipate. Cancer Cell *21*, 297–308.

Watts, J.L. (2009). Fat synthesis and adiposity regulation in *Caenorhabditis elegans*. Trends Endocrinol. Metab. *20*, 58–65.

Watts, J.L., and Browse, J. (2000). A palmitoyl-CoA-specific delta9 fatty acid desaturase from *Caenorhabditis elegans*. Biochem. Biophys. Res. Commun. *272*, 263–269.

Wilczynska, A., and Bushell, M. (2015). The complexity of miRNA-mediated repression. Cell Death Differ. *22*, 22–33.

Xu, J., Peng, W., Sun, Y., Wang, X., Xu, Y., Li, X., Gao, G., and Rao, Z. (2012). Structural study of MCPIP1 N-terminal conserved domain reveals a PIN-like RNase. Nucleic Acids Res. *40*, 6957–6965.

Yokogawa, M., Tsushima, T., Noda, N.N., Kumeta, H., Enokizono, Y., Yamashita, K., Standley, D.M., Takeuchi, O., Akira, S., and Inagaki, F. (2016). Structural basis for the regulation of enzymatic activity of Regnase-1 by domain-domain interactions. Sci. Rep. *6*, 22324.

Younce, C.W., Azfer, A., and Kolattukudy, P.E. (2009). MCP-1 (monocyte chemotactic protein-1)-induced protein, a recently identified zinc finger protein, induces adipogenesis in 3T3-L1 pre-adipocytes without peroxisome proliferator-activated receptor gamma. J. Biol. Chem. *284*, 27620–27628.